There is Plenty of Room for THz Tunneling Electron Devices Beyond the Transit Time Limit

Matteo Villani, Simone Clochiatti, Werner Prost, Nils Weimann, *Member, IEEE*, and Xavier Oriols, *Member, IEEE*

***Abstract*— The traditional transmission coefficient present in the original Landauer formulation, which is valid for quasi-static scenarios with working frequencies below the inverse of the electron transit time, is substituted by a novel time-dependent displacement current coefficient valid for frequencies above this limit. Our model captures in a simple way the displacement current component of the total current, which at frequencies larger than the inverse of the electron transit time can be more relevant than the particle component. The proposed model is applied to compute the response of a resonant tunneling diode from 10 GHz up to 5 THz. We show that tunneling electron devices are intrinsically nonlinear at such high frequencies, even under small-signal conditions, due to memory effects related to the displacement current. We show that these intrinsic nonlinearities (anharmonicities) represent an advantage, rather than a drawback, as they open the path for tunneling devices in many THz applications, and avoid further device downscaling.**

***Index Terms*— Displacement current, Landauer model, resonant tunneling diode, THz technologies.**

I. Introduction

FOR high enough frequencies, it is said that electron devices behave as low pass filters. This behavior starts beyond the so-called transit time limit. Microscopically, this limit is reached when electrons crossing the device are not affected by a static potential, but a time-dependent one. The usual strategy to design electron devices working at high frequencies is reducing their size to obtain smaller transit times.

Manuscript received December 24, 2020; accepted January 1, 2021. Date of publication January 5, 2021; date of current version January 27, 2021. This work was supported in part by Spain's Ministerio de Ciencia, Innovacion y Universidades (MCIU) [Agencia Estatal de Investigacion (AEI)/Fondo Europeo de Dessarollo Regional (FEDER), European Union (EU)] under Grant RTI2018-097876-B-C21, in part by the Generalitat de Catalunya and FEDER for QUANTUMCAT under Project 001-P-001644, in part by the Deutsche Forschungsgemeinschaft within the Collaborative Research Center SFB/TRR 196MARIE under Project C02, and in part by the European Union's Horizon 2020 Research and Innovation Programme GrapheneCore3 under Grant 881603 and the Marie Skłodowska-Curie TeraApps Grant 765426. The review of this letter was arranged by Editor V. Moroz. *(Corresponding author: Xavier Oriols.)*

Matteo Villani and Xavier Oriols are with the Department of Electronic Engineering, Universitat Autònoma de Barcelona, 08193 Bellaterra, Spain (e-mail: xavier.oriols@uab.es).

Simone Clochiatti, Werner Prost, and Nils Weimann are with the Components for High Frequency Electronics (BHE), University of Duisburg-Essen, 47057 Duisburg, Germany.

Digital Object Identifier 10.1109/LED.2021.3049229

We argue in this work that there is plenty of room for quantum devices to reach higher working frequencies (without further miniaturization) by designing them to work beyond the transit time limit. Beyond such limit, the output signal is not able to exactly follow the input signal, this produces nonlinearities that can be an advantage (rather than a drawback) for many applications like frequency multipliers, rectifiers, oscillators, and in general any signal modulator. Indeed, there are already prototypes of resonant tunneling diodes (RTD) as THz devices working at output frequencies close [1]–[4] or even beyond [5], [6] the mentioned transit time limit.

The THz nonlinearity (anharmonicity) that will be shown in this work appears in any ballistic device, as it needs to avoid the randomness due to collisions in the active region. Tunneling devices are chosen in this work, since they offer enriched quantum coherent electron dynamics by engineering the active region under AC conditions. We stress that the THz nonlinearity discussed in this work is unrelated to any nonlinearity present in the static characteristics of RTD devices.

The Landauer formula [7] based on the transmission coefficient has been a very simple and powerful tool to predict the response of tunneling devices below the transit time limit. Beyond the transit time limit, the displacement current component is known to become relevant over the particle one. This contribution has been modeled previously using a master equation [8] or a scattering matrix [9], [10] to deal with electron transitions between different parts of the tunneling device. In this work the electron is evolving in the whole tunneling structure, while keeping its full-coherence [11]–[13].

A simple, general and accurate model is presented for the computation of the total current in quantum coherent devices that just substitutes the traditional static transmission coefficient of the Landauer formula with the time-dependent displacement current coefficient. The model presented here, by construction valid beyond the transit time limit, shall spread the message of the title of this paper, opening intuition for quantum engineers to use the displacement current for new THz applications in electron tunneling devices.

II. Displacement Current Coefficient

We consider in this work a two-terminal device with an active region of length $L = b - a$ defined as the space between source and drain contacts ($a < x < b$). For DC computations,

the *transmission coefficient* T of the $i-$th electron injected from the left ($x < a$), at time t_i, is expressed by,

$$T = \int_b^{\infty} |\psi_i(x, t_i + \tau')|^2 \, dx = \int_{t_i}^{t_i+\tau'} J_i(b, t) dt \qquad (1)$$

where $|\psi_i(x,t)|^2$ is the quantum probability distribution of a wave-packet, $J_i(b,t)$ is the associated current density as defined in [14] calculated at the drain contact surface $x = b$. Finally τ' is a time interval large enough to ensure that the i-th electron has completely crossed the active region. Notice that we do not need to anticipate which is the exact electron transit time τ (which can be larger than the tunneling time [15], [16]) in Eq. 1 because the same value T will be obtained with whatever τ' satisfying $\tau' > \tau$ (for example $\tau' \to \infty$). To capture the dynamic behavior of electrons in THz scenarios, a Bohmian approach is here used [17]–[19] where each electron is described by a defined trajectory $x_i(t)$. The total current measured at the contacts of a two-terminal device is described by the Ramo-Shockley theorem [20], [21] as

$$I(t) = \frac{q}{L} \sum_{i=1}^{N(t)} v_i(x_i(t), t) \qquad (2)$$

where q is the electron charge and $N(t)$ is the number of electrons inside the device. The velocity $v_i(x,t) = J_i(x,t)/|\psi_i(x,t)|^2$ of each electron $x_i(t)$ is calculated [17], [18] from the wavepacket $\psi_i(x,t)$. We can see that (2) takes into account the displacement current because the movement of any $i-$th electron with $x_i(t) \in [a,b]$ contributes to the total current at time t (by generating a time-dependent electrical field everywhere [20]).

The parameter $N(t)$ does not need an explicit calculation because the number of electrons inside the active region given by the sum in (2) can be transformed into an integral over the probability of presence in the active region at time t for every i-th electron entering at time $t_i < t$. In other words: $\sum_{i=1}^{N(t)} \to \int_{t-\tau'}^{t} \gamma \, dt_i \int_a^b |\psi_i(x,t)|^2 \, dx$ where γ is a parameter proportional to the lateral area of the device [12]. Ignoring the energy integrals in the evaluation of the current (that would only obscure the conceptual discussion of this paper), the total current in (2) can be written as $I^f(t) = qD^f(t)$ with the *displacement current coefficient* given by

$$D^f(t) \equiv \frac{\gamma}{L} \int_{t-\tau'}^{t} dt_i \int_a^b dx \, J_i^f(x,t) = \int_{t-\tau'}^{t} dt_i G^f(t, t_i) \qquad (3)$$

The exact evaluation of $D^f(t)$ in Eq. (3) is as follows:

- The i-th electron is represented by an initial Gaussian wavepacket $\psi_i(x, t_i)$ at time t_i located outside of the active region.
- The time-dependent Schrödinger equation with a potential profile oscillating at frequency f is solved to get $\psi_i(x,t)$ and $J_i^f(x,t)$ at all times $[t_i, t_i + \tau']$.
- The contribution of the i-th electron to $D^f(t)$ evaluated from (3) is proportional to the amount of current density $J_i^f(x,t)$ inside the active region at time t.

The above three steps are repeated for the train of electrons with identical properties but different injecting times in the range $t_i \in [t, t - \tau']$. The injection time t_i is considered a continuous variable with a numerical discretization for practical computation. The $G^f(t, t_i)$ captures the "memory" effects and it quantifies the contribution of the i-th electron entering at t_i on the total current at time t for the external input frequency f. We specify again that no value of the exact electron transit time τ is needed in the computation of Eq. 3. In fact, the same value $D^f(t)$ will be obtained for any value of τ' as far as it satisfies $\tau' > \tau$. A reasonable estimation of the physical transit time of the i-th electron can be obtained by the usual expression $\tau = \int_{t_i}^{t_i+\tau'} dt \int_a^b dx |\psi_i(x,t)|^2$ with $\tau' > \tau$.

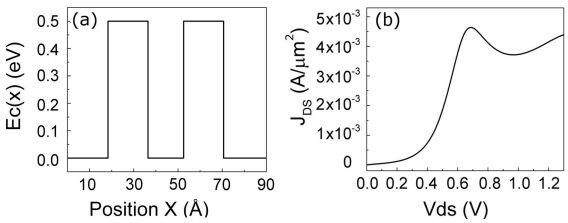

Fig. 1. (a) Band structure of GaAs/AlGaAs RTD device with 1.7 nm for both, barrier thickness and well width. (b) DC I-V characteristic of the RTD device.

III. Small-Signal and THz Nonlinearity in Time

In a quasi-static discussions of device performance, only the input signal amplitude becomes relevant to determine a linear behavior. We anticipate that linearity in our high frequency discussion will depend also on the input frequency f. The same small input signal amplitude that gives a linear behavior at a given low frequency can provide a non-linear one at higher frequency. In this section, we compute the time-dependent total current $I(t)$ for a RTD device whose potential profile $E_c(x)$ at zero bias is plotted in Fig. 1 together with its typical [1] DC characteristic with a current peak at $0.75\,V$.

A signal $V_{in}(t) = V_0 \, cos(2\pi f t + \phi)$ is applied at the drain (with the source contact grounded) with $V_0 = 0.01\,V$, which is a small enough value to have a linear I-V relationship. The time-dependent potential profile given by $E_c(x,t) = E_c(x) - x \cdot q \frac{V_0}{L} cos(2\pi f t + \phi)$ is considered, with ϕ the phase of the V_{in} signal. A non self-consistent potential profile is simulated, to avoid complications that will not change the main result of this work. It is worth underlining that the time dependent Schrödinger equation giving the evolution of the wavepackets $\psi_i(x,t)$ and $J_i^f(x,t)$ to compute $D^f(t)$ in Eq. 3 is driven by the time dependent Hamiltonian $H(x,t) = -\frac{\hbar^2}{2m}\frac{\partial^2}{\partial x^2} + E_c(x,t)$ which has no energy eigenstates because the electron total energy can vary locally during the electron transit along the active region. Certainly, such electron dynamics cannot be reached with the energy eigenstates linked to the time-independent Hamiltonians used in the Landauer model.

The result in Fig. 2 (a) shows the $D^f(t)$ coefficient for low input frequency of 10 GHz, here the response is linear because $f \ll 1/\tau$. For Fig. 2 (b)-(e), the nonlinear response can be seen in time domain. Frequency multiplication is observed in Fig. 2 (b)-(d) and confirmed in Fig. 2 (f), where the Power Spectral Density (PSD) of (a)-(d) is shown for every input frequency f. We recall that small signal conditions around zero bias are applied so that the nonlinearities are not due to the DC characteristics of the RTD exhibiting strong nonlinearity in Fig. 1. The nonlinearity originates from the fact that the i-th electron entering inside the device at time $t_i \approx t - \tau$ and another i'-th electron entering at time $t_{i'} \approx t$ are

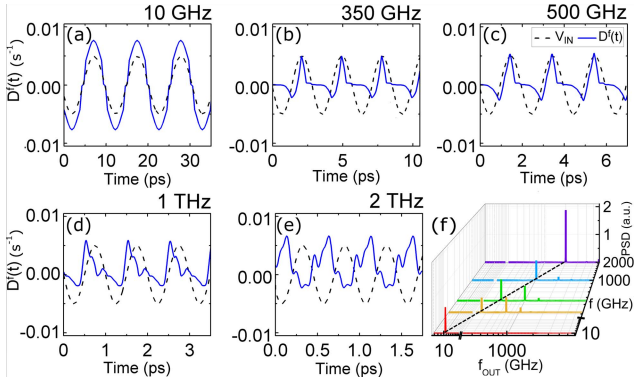

Fig. 2. (a)-(e) The displacement current coefficient $D^f(t)$, proportional to the output current I(t), is plotted (in blue) as a function of time for different input frequencies f, with the input small-signal AC voltage $V_{in}(t)$ (dashed black in arbitrary units). (f) Power spectral density (PSD) of the output currents of (a)-(e) as a function of the output frequency f_{out} confirming the harmonic generation of a nonlinear response.

affected by different potential profiles during their evolution. This produces different contributions to the total current $I(t)$ in Eq. 2. In other words, the quantum coherence of electron and displacement current ensure that the current $I(t)$ at time t is influenced not only by the potential profile $E_c(x,t)$, but also by $E_c(x,t-\tau)$. This is the "memory" effect leading to nonlinearity for high input frequency, even when a very small amplitude of the input signal is used.

IV. Small-Signal THz Nonlinearity in Frequency

We investigate now the same small-signal nonlinear RTD response in the frequency domain. If the RTD were a linear system, then when it is excited by a steady-state sinusoidal signal with frequency f, the output would be a sinusoidal signal with the same output frequency $f_{out} = f$ but different amplitude and phase. These would be described by a small signal conductance $Y_{11}(f)$ given by $I_R^f(t) + j \cdot I_I^f(t) = V_0\, Y_{11} \cdot e^{j2\pi f\, t}$, with $I_R^f(t)$ and $I_I^f(t)$ the real and imaginary components of the response to the small-signal $V_0 \cdot e^{j2\pi f\, t}$. See [23] for further details. We now explicitly rewrite the real part of the input signal $V_0\, cos(2\pi f\, t)$ and the imaginary part $V_0\, cos(2\pi f\, t - \pi/2)$. Then, using $I^f(t) = q D^f(t)$, one gets:

$$Y_{11} = \frac{I_R^f(0)}{V_0} + j\frac{I_I^f(0)}{V_0} = q\left(\frac{D_0^f}{V_0} + j\frac{D_{-\pi/2}^f}{V_0}\right) \qquad (4)$$

where the subindex $\phi = 0$ and $\phi = -\pi/2$ indicates the two phases (cosine and sine respectively) corresponding to the real and imaginary parts of the input signal. To simplify the notation, if $t = 0$, the t in $D^f(t)$ and $G^f(t,t_i)$ from Eq. 3 will be omitted.

In Fig. 3, the Y_{11} parameter defined in Eq. 4 is plotted. The behavior between 50 GHz and 300 GHz of the real (blue) and imaginary (red) components of Y_{11} is similar to the response of a device with a delay due to the transit (or switching) time τ [24]. In fact, it can be shown that our model exactly reproduces the Landauer model when $f \ll 1/\tau$. In this quasi-static regime, it can be shown that $D^f(t) = 1/L \int_a^b dx \int_{t-\tau}^t \gamma\, J_i(x, t-t_i) dt_i = \gamma\, T$. The results in Fig. 3 are related to the PSD shown in Fig. 2(f) by the dashed black line at $f_{out} = f$. With the small amplitude condition applied here, in principle, a linear response could be expected. However, it can be proved that this is not

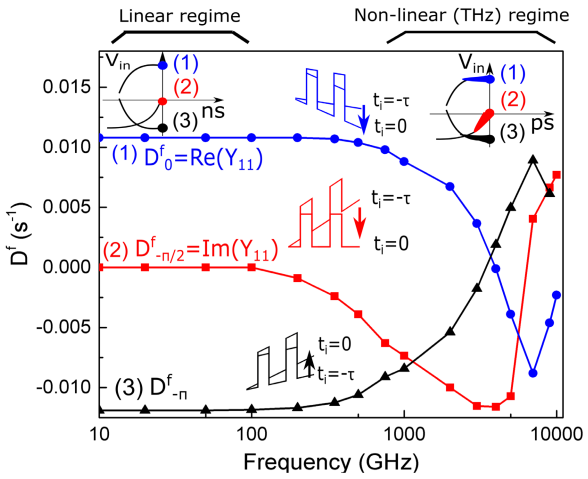

Fig. 3. The displacement current coefficient D^f of the RTD with an input signal $V_{in}(t)$ for different frequencies f estimated at phases: $\phi = 0$ (blue line), $\phi = -\pi/2$ (red line) and $\phi = -\pi$ (black line). For each phase, the evolution of the potential profile $E_C(x,t)$ of the RTD is shown. The left and right top insets show in black the input signal *before* the present time t for each of the three phases, and in colors the relevant times involved in the evaluation of D^f for low and high frequencies respectively. Linear regime (top-left inset) is achieved when the signal value $V_{in}(t_i)$ at $t_i \approx t-\tau$ is equal to the one at the present time t, whereas a nonlinear regime (top-right) is reached when $V_{in}(t-\tau) \neq V_{in}(t)$.

the case simply by computing the output current related to the input signal $V_0\, cos(2\pi f\ t - \pi)$, estimated with $D_{-\pi}^f$ plotted in black in Fig. 3. For a linear small signal device, one would expect $D_{-\pi}^f = -D_0^f$ because the input signals satisfy $cos(2\pi f\ t - \pi) = -cos(2\pi f\ t)$. This is true at low frequencies but at $f > 200$ GHz differences appear, proving nonlinearity. The frequency range $f > 200$ GHz is recently being explored for real RTD-based THz sources and detectors [2]–[4]. The physical and unavoidable reason of this small-signal nonlinearity at $f > 200$ GHz is explained by the function $G^f(t_i)$ in Eq. 3 and the evolution of the energy potential profiles plotted in the insets of Fig. 3. It can be seen how electrons injected at $t_i = -\tau$ travel faster under the (blue) potentials linked to $G_0^f(-\tau)$ than under the (black) potentials linked to $G_{-\pi}^f(-\tau)$. The blue potentials accelerate electrons due to $E_c(x,-t_i) > E_c(x,0)$, while the black potentials decelerate them due to $E_c(x,-t_i) < E_c(x,0)$. It follows that, the memory-related effects appear at smaller frequencies for $D_{-\pi}^f$ (as low as 100 GHz) than for D_0^f, as seen in Fig. 3.

V. Conclusion

In this paper, we present a model that substitutes the transmission coefficient in the Landauer formula by a new displacement current coefficient to capture realistic predictions of the behavior of tunneling devices at frequencies comparable or higher than the electron transit time (where the displacement current matters). The model is then used to show the nonlinear or anharmonic behavior of an RTD device in small signal condition around zero bias in a frequency window from 200 GHz to 5 THz. This frequency regime is here defined as the nonlinear (THz) regime, and it remains mainly unexplored by the scientific community. We argue that, depending on the proper engineering of the device that tailors the displacement current coefficient, different THz applications can be envisioned, as frequency multipliers, rectifiers, oscillators, modulators etc.

REFERENCES

[1] E. R. Brown, J. R. Söderström, C. D. Parker, L. J. Mahoney, K. M. Molvar, and T. C. McGill, "Oscillations up to 712 GHz in InAs/AlSb resonant-tunneling diodes," *Appl. Phys. Lett.*, vol. 58, no. 20, pp. 2291–2293, May 1991, doi: 10.1063/1.104902.

[2] J. Wang, K. Alharbi, A. Ofiare, H. Zhou, A. Khalid, D. Cumming, and E. Wasige, "High performance resonant tunneling diode oscillators for THz applications," in *Proc. IEEE Compound Semiconductor Integr. Circuit Symp. (CSICS)*, New Orleans, LA, USA, Oct. 2015, pp. 1–4, doi: 10.1109/CSICS.2015.7314509.

[3] K. Arzi, S. Clochiatti, S. Suzuki, A. Rennings, D. Erni, N. Weimann, M. Asada, and W. Prost, "Triple-barrier resonant-tunnelling diode THz detectors with on-chip antenna," in *Proc. 12th German Microw. Conf. (GeMiC)*, Stuttgart, Germany, Mar. 2019, pp. 1–18, doi: 10.23919/GEMIC.2019.8698124.

[4] T. Shiode, T. Mukai, M. Kawamura, and T. Nagatsuma, "Giga-bit wireless communication at 300 GHz using resonant tunneling diode detector," in *Proc. Asia–Pacific Microw. Conf.*, Melbourne, VIC, Australia, Dec. 2011, pp. 1122–1125.

[5] M. Feiginov, H. Kanaya, S. Suzuki, and M. Asada, "Operation of resonant-tunneling diodes with strong back injection from the collector at frequencies up to 1.46 THz," *Appl. Phys. Lett.*, vol. 104, no. 24, Jun. 2014, Art. no. 243509, doi: 10.1063/1.4884602.

[6] T. Maekawa, H. Kanaya, S. Suzuki, and M. Asada, "Oscillation up to 1.92 THz in resonant tunneling diode by reduced conduction loss," *Appl. Phys. Exp.*, vol. 9, no. 2, Jan. 2016, Art. no. 024101, doi: 10.7567/APEX.9.024101.

[7] R. Landauer, "Electrical resistance of disordered one-dimensional lattices," *Philos. Mag.*, vol. 21, no. 172, pp. 863–867, Apr. 1970, doi: 10.1080/14786437008238472.

[8] M. N. Feiginov, "Displacement currents and the real part of high-frequency conductance of the resonant-tunneling diode," *Appl. Phys. Lett.*, vol. 78, no. 21, pp. 3301–3303, May 2001, doi: 10.1063/1.1372357.

[9] Y. M. Blanter and M. Büttiker, "Shot noise in mesoscopic conductors," *Phys. Rep.*, vol. 336, nos. 1–2, pp. 1–166, Sep. 2000, doi: 10.1016/S0370-1573(99)00123-4.

[10] Y. V. Nazarov and Y. M. Blanter, *Quantum Transport: Introduction to Nanoscience*. Cambridge, U.K.: Cambridge Univ. Press, May 2009, pp. 29–41.

[11] M. Villani, X. Oriols, S. Clochiatti, N. Weimann, and W. Prost, "The accurate predictions of THz quantum currents requires a new displacement current coefficient instead of the traditional transmission one," in *Proc. 3rd Int. Workshop Mobile THz Syst. (IWMTS)*, Essen, Germany, Jul. 2020, pp. 1–5, doi: 10.1109/IWMTS49292.2020.9166410.

[12] E. Fernandez-Diaz, A. Alarcon, and X. Oriols, "Modeling quantum transport under AC conditions: Application to intrinsic high-frequency limits for nanoscale double-gate Si MOSFETs," *IEEE Trans. Nanotechnol.*, vol. 4, no. 5, pp. 563–569, Sep. 2005, doi: 10.1109/TNANO.2005.851407.

[13] X. Oriols, "Quantum-trajectory approach to time-dependent transport in mesoscopic systems with electron-electron interactions," *Phys. Rev. Lett.*, vol. 98, no. 6, Feb. 2007, Art. no. 066803, doi: 10.1103/PhysRevLett.98.066803.

[14] C. Cohen-Tannoudji, B. Diu, and F. Laloë, *Quantum Mechanics: Basic Concepts, Tools, and Applications*, vol. 1, 1st ed. New York, NY, USA: Wiley, Jun. 1978, p. 239.

[15] R. Landauer and T. Martin, "Barrier interaction time in tunneling," *Rev. Mod. Phys.*, vol. 66, no. 1, pp. 217–228, Jan. 1994, doi: 10.1103/RevModPhys.66.217.

[16] A. S. Landsman and U. Keller, "Attosecond science and the tunnelling time problem," *Phys. Rep.*, vol. 547, pp. 1–24, Jan. 2015, doi: 10.1016/j.physrep.2014.09.002.

[17] D. Bohm, "A suggested interpretation of the quantum theory in terms of 'hidden' variables. I," *Phys. Rev.*, vol. 85, no. 2, pp. 166–179, Jan. 1952, doi: 10.1103/PhysRev.85.166.

[18] X. Oriols and J. Monpart, *Applied Bohmian Mechanics: From Nanoscale Systems to Cosmology*, 2nd ed. Singapore: Jenny Stanford Publishing, May 2019, pp. 15–101, doi: 10.1201/9780429294747.

[19] D. Marian, N. Zanghì, and X. Oriols, "Weak values from displacement currents in multiterminal electron devices," *Phys. Rev. Lett.*, vol. 116, no. 11, Mar. 2016, Art. no. 110404, doi: 10.1103/PhysRevLett.116.110404.

[20] S. Ramo, "Currents induced by electron motion," *Proc. IRE*, vol. IRE-27, no. 9, pp. 584–585, Sep. 1939, doi: 10.1109/JRPROC.1939.228757.

[21] W. Shockley, "Currents to conductors induced by a moving point charge," *J. Appl. Phys.*, vol. 9, no. 10, pp. 635–636, Oct. 1938, doi: 10.1063/1.1710367.

[22] F. L. Traversa, Z. Zhan, and X. Oriols, "Absorption and injection models for open time-dependent quantum systems," *Phys. Rev.*, vol. 90, no. 2, Aug. 2014, Art. no. 023304, doi: 10.1103/PhysRevE.90.023304.

[23] S. E. Laux, "Techniques for small-signal analysis of semiconductor devices," *IEEE Trans. Electron Devices*, vol. ED-32, no. 10, pp. 2028–2037, Oct. 1985, doi: 10.1109/T-ED.1985.22235.

[24] Z. Zhan, E. Colomés, and X. Oriols, "Limitations of the intrinsic cutoff frequency to correctly quantify the speed of nanoscale transistors," *IEEE Trans. Electron. Devices*, vol. 64, no. 6, pp. 2617–2624, Jun. 2017, doi: 10.1109/TED.2017.2691400.